Electronic Supplementary Material (ESI) for Nanoscale.

Supplementary Information

Gap States Distribution and Fermi Level Pinning in Monolayer to Multilayer MoS_2 Field Effect Transistors

Ronen Dagan[*,‖,⊥] **, Yonatan Vaknin**[‖,⊥]**, and Yossi Rosenwaks**[*,‖]

‖ School of Electrical Engineering, Tel-Aviv University, Tel Aviv 69978, Israel.

Appendix A

Electrical measurements were conducted using a semiconductor parameter analyser (*B1500A, Agilent Technologies*). Drain current as a function of the back-gate voltage is shown on the left for each sample, while drain current as a function of drain voltage is on the right.

(a) Monolayer

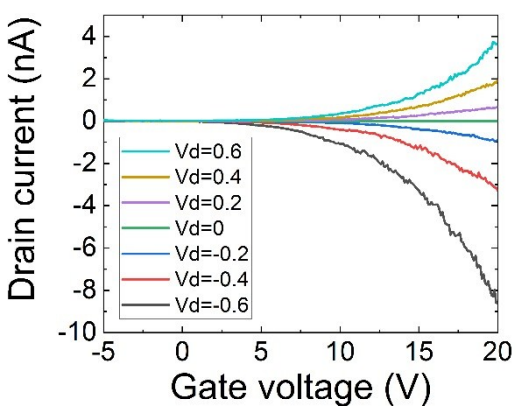

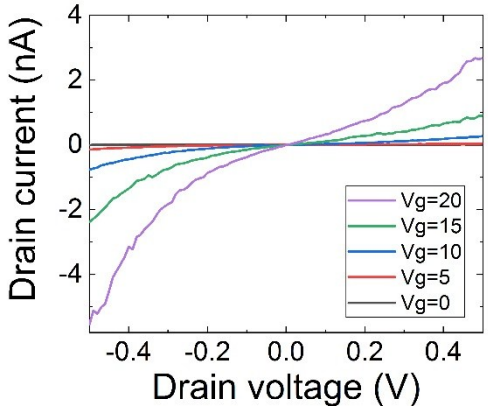

(b) Bilayer

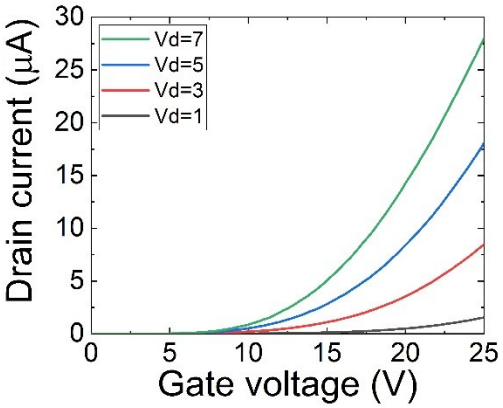

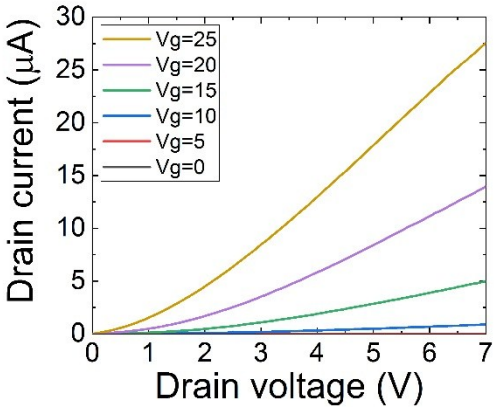

(c) Few layers

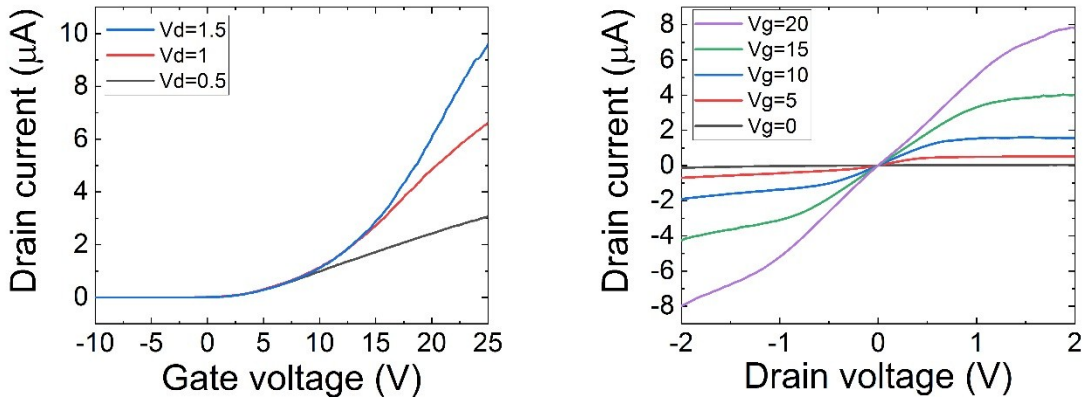

Supplementary Figure S1. *Electrical characteristics for (a) monolayer, (b) bilayer, and (c) few layered device, used for understanding the gate, source-drain voltages range, which operates the device in the different regimes, as well as assessing the contacts quality.*

KPFM measurements were performed in the "dual frequency" configuration, where the topography is recorded at the fundamental resonance frequency of the tip, and the surface potential is measured at its second harmonic using a single pass. Figure S2 presents the surface potential cross sections taken between source and drain, where source and drain electrodes were grounded, and the back-gate voltage was modified. These plots were used to determine the Fermi level shift as a response to each applied back-gate bias. It was later used in the gap-states analysis, described in details in appendix B.

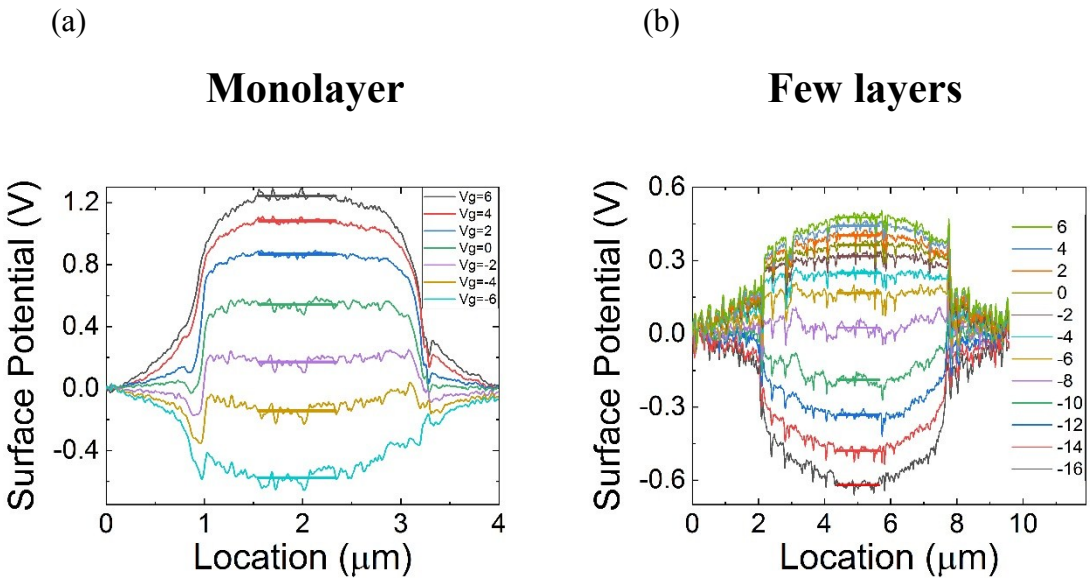

Supplementary Figure S2. *Surface potential measurements at varying back-gate voltages while* $V_S = V_D = 0\,V$*, for (a) monolayer, and (b) few layers. The bold lines represent the average surface potential over the* MoS_2 *film, away from the grounded metal contacts.*

In order to assess the effective back-gate potential reaching the MoS_2, after the voltage drop on the oxide, together with the voltage drop on the MoS_2 itself (for agreement with the KPFM tip, which measure the potential at the MoS_2/air interface) - a proper finite element simulation was conducted. The results for the Few-layered sample are shown below, while for the bilayer in Figure 2d.

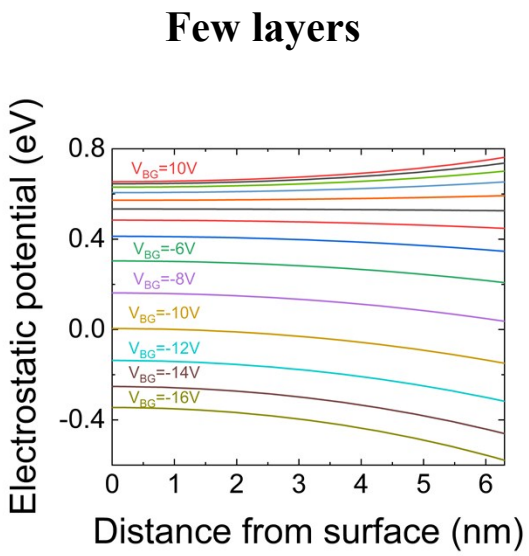

Supplementary Figure S3. *A cross-sectional electrostatic potential drop, from the MoS_2/oxide interface at the right side of the figure, through the MoS_2 channel, up to the air/MoS_2 interface at the left side of the figure, for gate bias range of 6 to -16V, extracted from the electrostatic simulation.*

A two-dimensional finite element simulation (Sentaurus TCAD, Version L-2016.03, Synopsys) of a bi-layer MoS_2 based FET-like structure, emulating the measured device at the same measuring conditions. An air gap of $200nm$ was added on top of the MoS_2 layer to enforce Neumann boundary conditions apart from the MoS_2 layer. Mid-gap traps were added to the simulated MoS_2 layer (including exponential tail close to the conduction band, a base uniform distribution, and several different mid-gap peaks), in order to track measured Fermi level shift as function of the applied back-gate voltage, at the upper interface of the device.

Regarding the way of distinguishing between FL pinning due to metal/semiconductor contact, or due to the GS at the semiconductor itself, we have fabricated and analysed many samples, some of which had significant FL pinning at the MoS_2/Au interface. As demonstrated below, our KPFM measurements can distinguish between FL pinning at the MoS_2/Au interfaces versus pinning by gap states the MoS_2 layer itself; consequently, all the measurements presented in the manuscript are of samples who had small FL pinning at the interface in order to focus on FL pinning at the MoS_2 layers.

The Figure below present raw data measured for samples with FL pinning at the MoS_2/Au contact (top), in comparison to FL pinning at the MoS_2 layer itself (bottom). The main difference

is that in the top Figure the measured surface potential (which is a direct measurement of the FL) at the two contacts (circled) hardly changes with applied bias- pinning, and there is no substantial pinning in the MoS_2 layer itself. The pinning is also evident by the non-ohmic IV characteristic on the right. In the bottom figure the pinning (although substantial) is governed by the MoS_2 layer and not by the contacts and the corresponding I-V is ohmic. Figure 2a in the manuscript represents a sample that is not significantly pinned both by the gap states and the contacts.

(a)

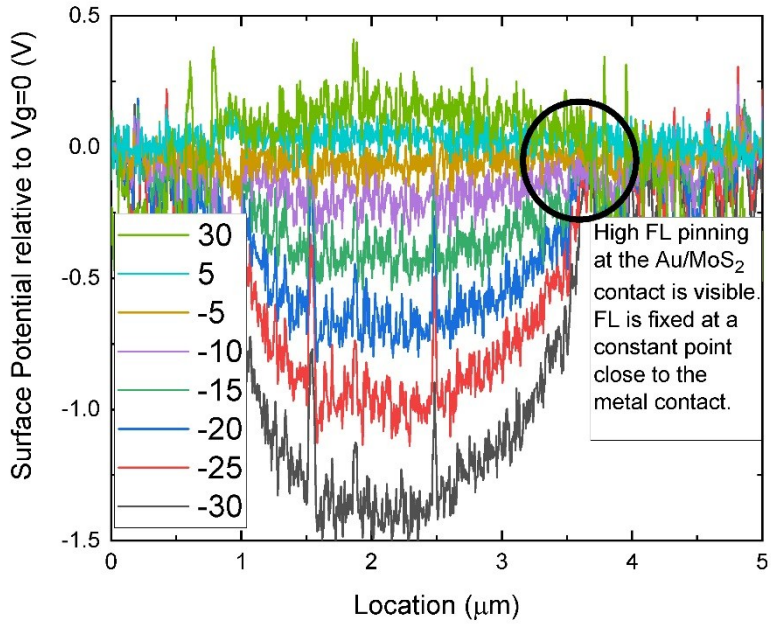

FL is pinned close to the contacts but is shifted by a large range ~1.5 eV far away from the metal/semiconductor junction.

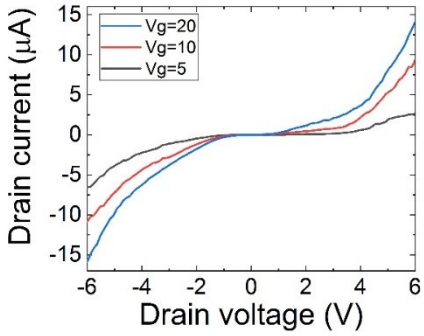

IV characteristics show clear schotky behavior.

(b)

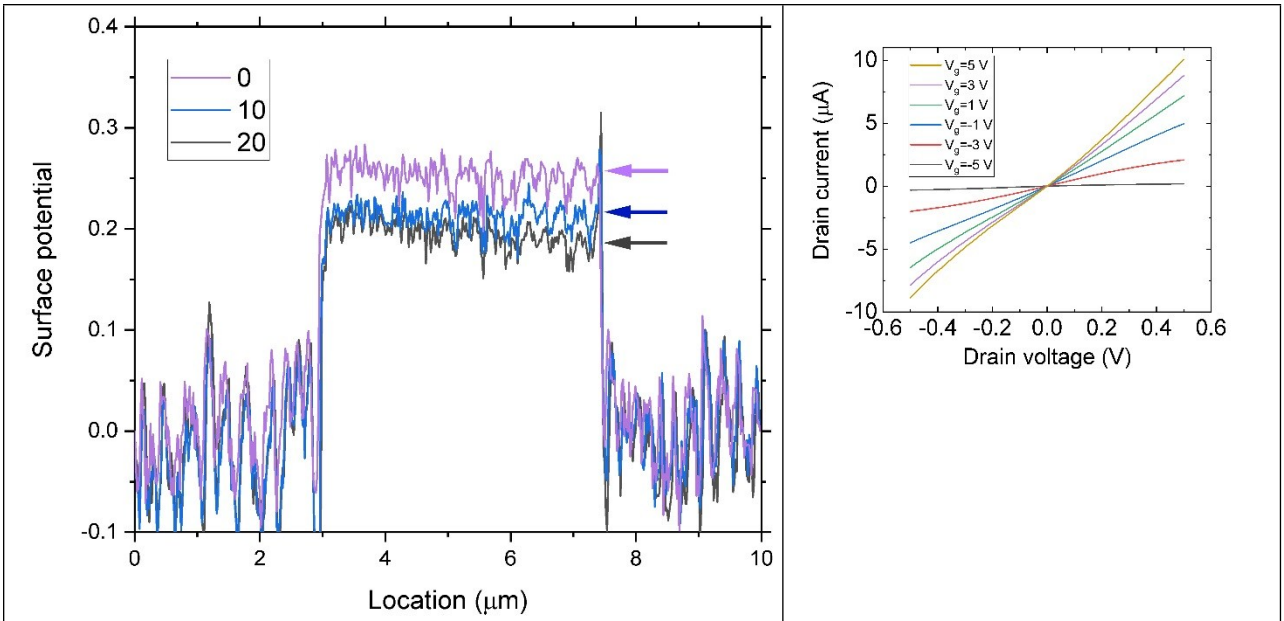

- FL is not pinned close to the contacts but is shifted in a very small range <0.1 eV, even far away from the metal/semiconductor junction.
- IV characteristics show ohmic behavior.

Supplementary Figure S4. *(a) Surface potential profiles and Schottky I-V characteristics for sample with FL pinning at the MoS_2/Au contact. (b) Surface potential profiles and ohmic I-V characteristics for sample with FL pinning at the MoS_2.*

(a) (b)

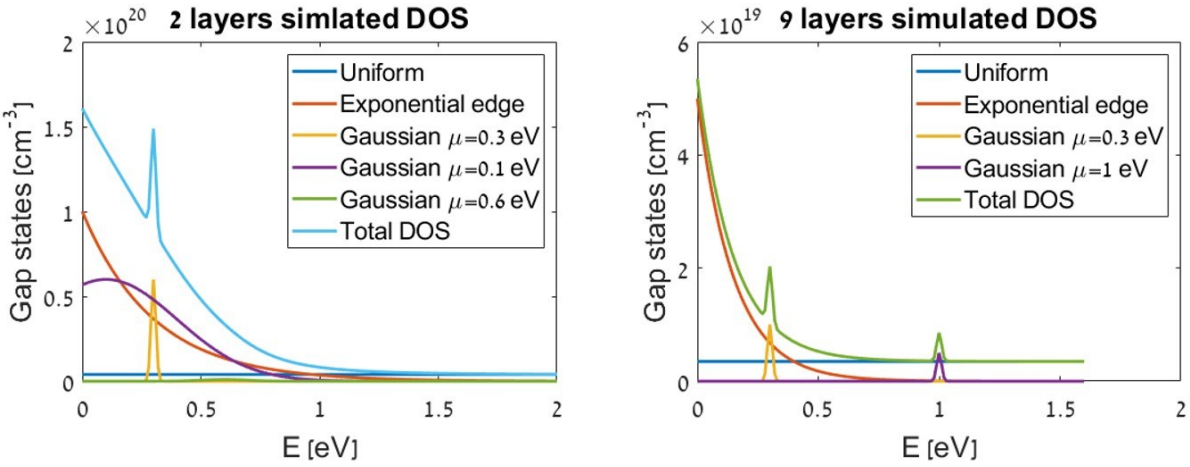

Supplementary Figure S5. *Simulated gap states distribution for (a) 2 layers, (b) 9 layers. Conduction bands were aligned to 0 eV.*

Appendix B

Extraction of the density of states

The charge concentration is given by:

$$n = \int_{-\infty}^{\infty} g(E) f_{FD}(E) dE$$

qV_L is defined as the shift of Fermi level with respect to E_F at the insulator-semiconductor interface. After differentiation by V_L we have:

$$\frac{dn}{dV_L} = \int_{-\infty}^{\infty} g(E) \frac{df_{FD}(E)}{dV_L} dE$$

On the right side of the equation, Fermi-Dirac distribution is given by:

$$f_{FD}(E, V_L) = \frac{1}{1 + \exp\left(\frac{E - E_F^t - qV_L}{kT}\right)}$$

Fermi-Dirac distribution as a function of V_L, at a constant Energy is shown below:

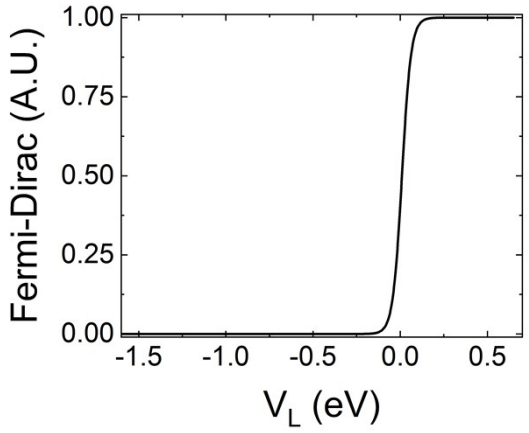

Supplementary Figure S6. Fermi-Dirac distribution as a function of V_L, at a constant Energy.

And its derivative with respect to V_L:

$$\frac{df_{FD}(E, V_L)}{dV_L} = \frac{q}{kT} \frac{\exp\left(\frac{E - E_F^t - qV_L}{kT}\right)}{\left[1 + \exp\left(\frac{E - E_F^t - qV_L}{kT}\right)\right]^2}$$

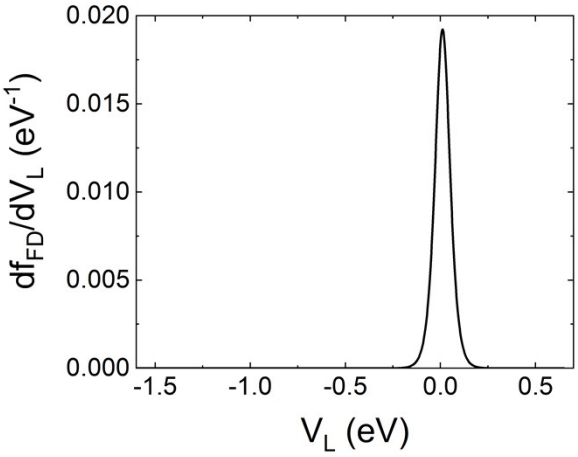

Supplementary Figure S7. *Derivative of Fermi-Dirac distribution with respect to* V_L*, at a constant Energy.*

When the width of $\frac{df_{FD}}{dV_L}$ is much narrower relative to that of $g(E)$ it can be approximated by a delta function:

$$\frac{\exp\left(\frac{E-E_F^t-qV_L}{kT}\right)}{\left[1+\exp\left(\frac{E-E_F^t-qV_L}{kT}\right)\right]^2}=\delta\left(\frac{E-E_F^t-qV_L}{kT}\right)$$

Inserting former equations we obtain:

$$\frac{dn}{dV_L}=\frac{q}{kT}\int_{-\infty}^{\infty}g(E)\delta\left(\frac{E-E_f^t-qV_L}{kT}\right)dE$$

Using $\delta\left(\frac{x}{a}\right)=a\delta(x)$ we have:

$$\frac{dn}{dV_L}=q\int_{-\infty}^{\infty}g(E)\delta\left(E-E_f^t-qV_L\right)dE$$

By applying $\int f(x)\delta(x-a)dx=f(a)$, we remain with:

$$\frac{dn}{dV_L}=qg(E_f^t+qV_L)$$

Thus the gap-states as a function of qV_L is:

$$g(E_f^t + qV_L) = \frac{1}{q}\frac{dn}{dV_L}$$

Finally, we apply: $n(x) = (C_{OX} / qd_{org})(V_{GS} - V_t - V_L(x))$ to remain with:

$$g(qV_L(x)) = \frac{C_{OX}}{d_{org}q^2}\left(\frac{dV_{GS}}{dV_L(x)} - 1\right)$$